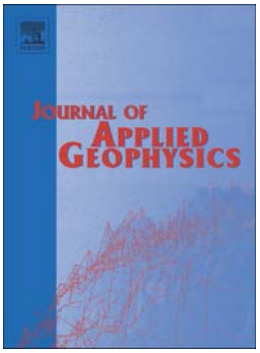

Near-surface fault detection by migrating back-scattered surface waves with and without velocity profiles

Han Yu, Yunsong Huang, Bowen Guo

PII: S0926-9851(16)30113-6
DOI: doi: 10.1016/j.jappgeo.2016.04.013
Reference: APPGEO 2978

To appear in: *Journal of Applied Geophysics*

Received date: 27 July 2015
Revised date: 13 April 2016
Accepted date: 23 April 2016

Please cite this article as: Yu, Han, Huang, Yunsong, Guo, Bowen, Near-surface fault detection by migrating back-scattered surface waves with and without velocity profiles, *Journal of Applied Geophysics* (2016), doi: 10.1016/j.jappgeo.2016.04.013

Near-surface Fault Detection by Migrating Back-scattered Surface Waves with and without Velocity Profiles

Han Yu [1], Yunsong Huang [2], and Bowen Guo [3]

[1] School of Computer Science and Technology, Nanjing University of Posts & Telecommunications, Nanjing 210023, China, Email: han.yu@njupt.edu.cn, Tel: +86-13951823250
[2] Subsurface Imaging, CGG, Houston, USA, Email: yunsong.huang@cgg.com
[3] Division of Physical Sciences and Engineering, King Abdullah University of Science and Technology, Thuwal 23955-6900, Saudi Arabia, Email: bowen.Guo@kaust.edu.cn

Abstract

We demonstrate that diffraction stack migration can be used to discover the distribution of near-surface faults. The methodology is based on the assumption that near-surface faults generate detectable back-scattered surface waves from impinging surface waves. We first isolate the back-scattered surface waves by muting or FK filtering, and then migrate them by diffraction migration using the surface wave velocity as the migration velocity. Instead of summing events along trial quasi-hyperbolas, surface wave migration sums events along trial quasi-linear trajectories that correspond to the moveout of back-scattered surface waves. We have also proposed a natural migration method that utilizes the intrinsic traveltime property of the direct and the back-scattered waves at faults. For the synthetic data sets and the land data collected in Aqaba, where surface wave velocity has unexpected perturbations, we migrate the back-scattered surface waves with both predicted velocity profiles and natural Green's function without velocity information. Because the latter approach avoids the need for an accurate velocity model in event summation, both the prestack and stacked migration images show competitive quality. Results with both synthetic data and field records validate the feasibility of this method. We believe applying this method to global or passive seismic data can open new opportunities in unveiling tectonic features.

Keywords: Back-scattered Surface Waves; Migration; Fault Detection; Velocity; Natural Green's Function

1. INTRODUCTION

Surveys in engineering and exploration are used to detect the distribution of near-surface faults. Accurate fault maps can be used to avoid unsafe construction of buildings or placement of drilling platforms. Detecting hidden faults near the surface can also be used to predict the optimal location of paleo seismic trench surveys that determine the magnitude and recurrence intervals of ancient earthquakes.

Shallow seismic surveys indirectly detect the presence of near surface faults by computing reflection sections, and inferring faults from the discontinuities of the

reflection horizons. This indirect procedure is often successful, but it requires careful processing of the data to extract the reflection events, estimation of the correct stacking velocity, and sometimes a rigorous estimate of the statics. Moreover, the very early arrivals are muted due to the limitations in source-receiver sampling, so the reflectors very close to the surface are ignored. Such ignorance might prevent the detection of faults within several wavelengths of the free surface. For interferometric processing of passive seismic data, body-wave reflections are very difficult to extract, especially from shallow layers.

This paper proposes the direct detection of near-surface faults by diffraction migration and natural migration of back-scattered surface waves. The faults are directly detected by migrating the back-scattered surface waves to their place of origin along the fault. The key assumption is that near-surface faults generate detectable back-scattered surface waves from impinging surface waves. This migration procedure is related to the interferometry method proposed by Schuster et al. (2012) except that the data are directly migrated, rather than interferometrically redatumed, for trial image points on the surface. The processing steps are to isolate the back-scattered surface wave events (Yu et al., 2014), and then to migrate them by diffraction migration using the surface wave velocity as the migration velocity. Instead of summing events along trial hyperbolas, surface wave migration sums events along trial quasi-linear trajectories that correspond to that of the backscattered surface waves. A deconvolution filter is also derived from the data, and it can collapse the dispersed surface wave arrival into a non-dispersive event whenever necessary. In this study, the velocity distribution is either a constant, or an estimated one by velocity scan, or not necessarily required for migration due to a proposed natural migration method by extracting Green's function from the data. Results with synthetic data and field records validate the feasibility of this method.

This paper is organized into four sections. The first part is the introduction, and the second part presents the theory. The third part shows numerical results with both synthetic data and field data. The field data are for a seismic survey over a desert region in Aqaba (Thuwal, Saudi Arabia) with faults at the near surface. The final section presents the conclusions.

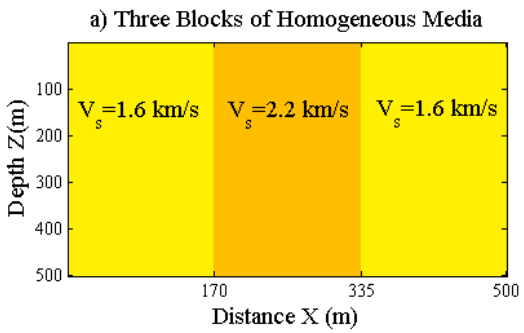

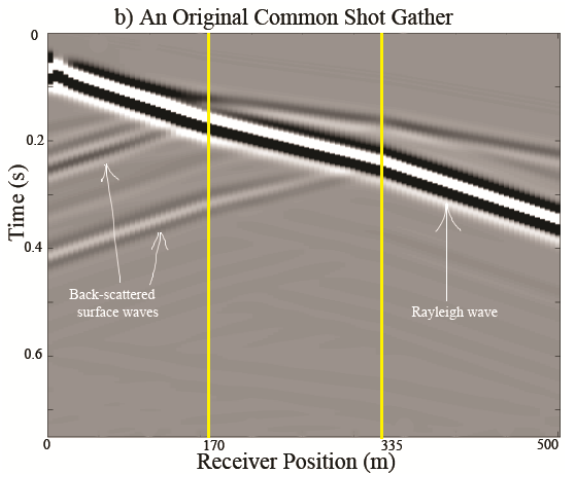

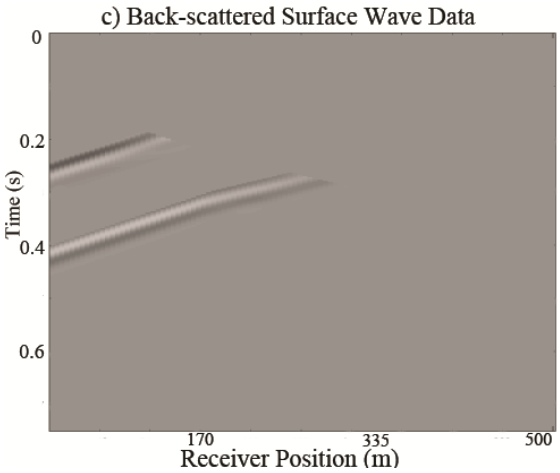

Figure 1: a) Three blocks of homogeneous media to generate surface waves, b) surface wave records for a vertical displacement point source at (x_s = 5 *m*, z_s = 0 *m*) and vertical component geophones on the free surface, c) the back-scattered surface waves after muting. The two vertical lines in Figure 1(a) are the faults that separate one velocity block from another. The two yellow vertical lines in Figure 1(b) mark the position of the two faults. The velocities determine those of the simulated Rayleigh waves.

2. THEORY OF SURFACE WAVE MIGRATION

2.1 MIGRATION OF BACK-SCATTERED SURFACE WAVES

The vertical-component particle velocity of a propagating Rayleigh wave over a homogeneous half space can be approximated by the Green's function

$$G(\mathbf{g}\,|\,\mathbf{s}) = W(\omega)\,A(\mathbf{g},\mathbf{s})\,e^{ik|\mathbf{g}-\mathbf{s}|}e^{-\kappa|z|}, \tag{1}$$

where the source at **s** and vertical-component particle-velocity geophone at **g** are both on the free surface (Aki and Richards, 1981), z is the depth, and κ is the vertical component of the wavenumber vector. The horizontal wavenumber is given by $k = \omega/c$, where c represents the Rayleigh wave velocity in a homogeneous medium (like one block in Figure 1(a)) and ω is the angular frequency of the vertical component point source on the free surface. The term $A(\mathbf{g}, \mathbf{s})$ takes into account the geometrical spreading of the surface wave from **s** to **g** and $W(\omega)$ is the source wavelet spectrum with the frequency ω that also includes a phase term associated with the Green's function for the surface wave; for convenience we will assume that this phase term is deconvolved from the data. The errors that the approximation makes largely attribute to the neglects of the radiation pattern and the body wave's contribution to the Green's function (Snieder, 1986). As an example, Figure 1(b) shows the simulated surface waves for a model with three homogeneous blocks of velocity. The back-scattered surface waves (Figure 1(c)) are the events that moveout in the opposite direction of the incident surface wave. These records are computed by a finite-difference solution to the 2D elastic wave equation (Virieux, 1986).

Previous work (Snieder, 1986; Blonk and Herman, 1994; Campman et al., 2003; van Wijk, 2003; Luke and Calderón-Macías, 2008) on imaging Rayleigh wave scattering from impedance discontinuities approximates the scattered waves at the free surface as a weighted surface integral of Green's tensors that take into account surface-wave propagation. The weights are impedance discontinuities s(**x**) on the free surface or very near the free surface and the integration is over the free surface; the impedance discontinuity can be considered to be a function of frequency to account for depth variations in the impedance function. The inverse to this integral equation gives the impedance distribution. In our proposal, we simply assume that the surface-wave response to an impedance discontinuity represented by a near-surface fault can be approximated by a surface integral of Green's functions weighted by the impedance discontinuity associated with the fault. Instead of inverting this equation in the least squares sense, we will simply apply its adjoint to the data to get the migration image on the surface.

The following steps are to migrate the back-scattered surface waves to their origin point along the fault near the surface. The important assumption is that the dominant back-scattered arrivals are from the near-surface portions of the fault. This assumption is reasonable and can be partly illustrated by a field data set in the next section.

1. We will assume that the traveltime of surface waves from **x** to **x**' at a specific frequency is given by $\tau_{\mathbf{x}\mathbf{x}'}$, where the traveltime does not dependence on frequency. If the subsurface is homogeneous then the velocity is independent of frequency, but if the Rayleigh wave is dispersive then we can perform migration in the frequency domain using the phase velocity as the migration velocity. Alternatively, we can assume that the dispersive wavelet has been compressed to a narrow wavelet using a suitable deconvolution filter, and errors due to the radiation patterns and converted waves of body waves are neglected. In this case the forward data can be approximated by equation 1 and the back-scattered surface waves $\underline{d}(\mathbf{x}|\mathbf{s})^{scatt}$ can be approximated by

$$\underline{d}\left(\mathbf{g}\,|\,\mathbf{s}\right)=W\left(\omega\right)A\left(\mathbf{s},\mathbf{x}_f\right)A\left(\mathbf{g},\mathbf{x}_f\right)re^{i\omega\left(\tau_{\mathbf{s}\mathbf{x}_f}+\tau_{\mathbf{g}\mathbf{x}_f}\right)},\mathbf{x}_\mathbf{g},\mathbf{x}_\mathbf{s}<\mathbf{x}_f\,, \tag{2}$$

where the back-scattered reflection coefficient is denoted by r, the vertical fault at $\mathbf{x}_f = (x_f, 0)$ is to the right of the source **s**, and the back-scattered field at $\mathbf{g} = (x_g, 0)$ is only alive to the left of the fault. Here, $A(\mathbf{g}, \mathbf{x}_f)$ accounts for geometrical spreading from the scatterer location at $\mathbf{x}_f$ to **g** at the left of the fault. The terms τ_{sx_f} and τ_{gx_f} respectively imply the traveltime of the propagating direct wave from the source to the fault, and the traveltime of the back-scattered wave from the fault to the geophone.

2. The back-scattered data $\underline{d}(\mathbf{g}|\mathbf{s})^{scatt}$ (x_g, $x_s < x_f$) are migrated using the diffraction stack migration formula

$$m\left(\mathbf{x}'\right)=\sum_{\mathbf{g}}\underline{d}\left(\mathbf{g}\,|\,\mathbf{s}\right)^{scatt}e^{-i\omega\left(\tau_{\mathbf{s}\mathbf{x}'}+\tau_{\mathbf{g}\mathbf{x}'}\right)}\hat{W}^{-1}\left(\omega\right),\mathbf{x}_\mathbf{g},\mathbf{x}_\mathbf{s}<\mathbf{x}', \tag{3}$$

where $m(\mathbf{x}')$ is the migration image at the trial image point $\mathbf{x}' = (x', 0)$ such that $\mathbf{x_g} < x'$ and $\hat{W}^{-1}(\omega)$ is the deconvolution filter that also accounts for possible dispersion effects. The condition $x_g, x_s < x_f$ indicates that the source and the receivers should stay in the same side to the possible fault. The term $\underline{d}'(\mathbf{x}|\mathbf{s})$ denotes the signal received at the possible fault position $\mathbf{x}'$; therefore, if there exists a fault at $\mathbf{x}$, then the back-scattered data $\underline{d}'(\mathbf{g}|\mathbf{s})^{scatt}$ can be recorded by the geophone at $\mathbf{g}$.

3. Plugging equation 2 into equation 3 gives

$$m(\mathbf{x}') = \sum_{\mathbf{g}} A(\mathbf{g},\mathbf{x}_f)\, A(\mathbf{s},\mathbf{x}_f)\, r e^{-i\omega\left(\tau_{\mathbf{sx}'} + \tau_{\mathbf{gx}'} - \tau_{\mathbf{sx}_f} - \tau_{\mathbf{gx}_f}\right)}, \tag{4}$$

with $\mathbf{x}_g, \mathbf{x}_s < \mathbf{x}'$. If $\mathbf{x}' = x_f$, then the migration formula becomes

$$m(\mathbf{x}') = \sum_{\mathbf{g}} A(\mathbf{g},\mathbf{x}_f)\, A(\mathbf{s},\mathbf{x}_f)\, r, \;\; \mathbf{x}_g, \mathbf{x}_s < \mathbf{x}', \tag{5}$$

which coherently sums over all frequencies. This formula provides the maximum amplitude in the migration image on the surface, and therefore pinpoints the location of the fault. If the fault does not break the free surface, then we can assume that the interaction of the surface wave with the near-surface fault generates a body wave that propagates from the buried fault to the surface, and transforms into a back-scattered surface wave. This extra time delay from the subsurface fault plane to the surface can be accounted for by an extra phase term $exp(-i\omega\tau_{\mathbf{x}'\mathbf{g}})$ in the migration kernel, which can be ignored if the fault is less than a quarter of a wavelength from the free surface. The geophone location $\mathbf{g}$ is restricted to be at locations directly above the scattering points along the fault. If the time delay cannot be ignored, then the trial image points should also be just below the free surface and the extra phase term should be incorporated into the migration operator. If the dispersion velocity $c(\omega)$ of the fundamental mode is estimated from the Rayleigh wave, then the deconvolution filter that compresses the dispersive Rayleigh wave to a compressed pulse propagating with velocity c_o is given by $\hat{W}^{-1}(\omega) = W^{-1}(\omega)\; exp\{-i\omega(\tau(\omega)_{xs} - |\mathbf{x}-\mathbf{s}|/c_o)\}$, where $\tau(\omega)_{\mathbf{xs}} = |\mathbf{x}-\mathbf{s}|/c(\omega)$. Here, $\mathbf{x}$ and $\mathbf{s}$ are on the free surface. The expression of $\hat{W}^{-1}(\omega)$ serves as a de-dispersion technique to add the energy of dispersive waves back to the Rayleigh wave of the fundamental mode. The phase velocity can be directly extracted from the data or it can be estimated by velocity scan acting on the surface waves.

4. The space-time version of the migration equation can be obtained by summing equation 3 over all frequencies to give

$$m(\mathbf{x}') = \sum_{\omega}\sum_{\mathbf{g}} \underline{d}(\mathbf{g}\,|\,\mathbf{s})^{scatt}\, e^{-i\omega\left(\tau_{\mathbf{sx}'}+\tau_{\mathbf{gx}'}\right)}\hat{W}^{-1}(\omega),$$
$$= \sum_{t}\sum_{\mathbf{g}} d\left(\mathbf{g}, \tau_{\mathbf{sx}'}+\tau_{\mathbf{gx}'}\,|\,\mathbf{s},0\right)^{scatt}, \qquad (6)$$

where $d(\mathbf{g}, \tau_{sx'}+\tau_{gx'}|\mathbf{s}, 0)$ is the deconvolved back-scattered surface wave data in the space-time domain at the listening time denoted by $\tau_{sx'}+\tau_{gx'}$. This listening time is physically interpreted as the quasi-linear moveout of the dominant portion of the back-scattered surface wave. In fact, it moves out with the group velocity if the dispersion effects have been properly deconvolved or filtered off. Alternatively, the data can be migrated in the frequency domain at the phase velocity of the surface wave. The summation over the horizontal geophone coordinates says that the migration image is obtained by summing the back-scattered surface wave data over trial quasi-linear curves in the data ($\mathbf{x}_g$–t) space associated with the trial image point at $\mathbf{x}' = (x', 0)$. Compared to reflection migration which sums the reflection data over trial quasi-hyperbola curves associated with the trial image point at $\mathbf{x}'$, such calculation can be more conveniently implemented.

2.2 MIGRATION WITH NATURAL GREEN'S FUNCTION

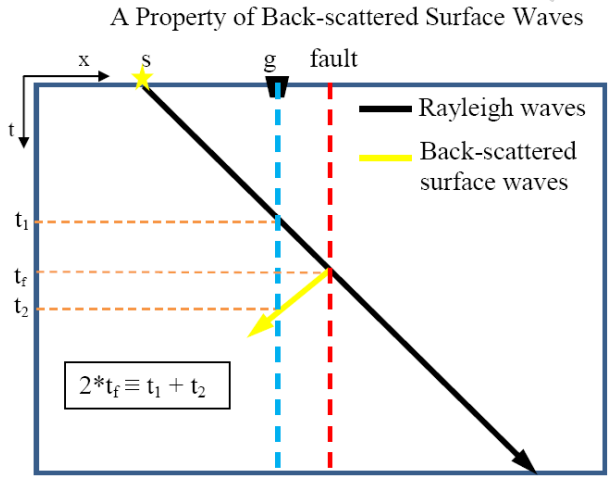

Figure 2: A property of back-scattered surface waves for natural migration.

We also propose to migrate a data set with natural Green's function using an important property of back-scattered surface waves. In the space-time data domain depicted by Figure 2, whenever a geophone **g** records back-scattered surface signals, the following relation holds regardless of the local velocity variations:

$$2t_f = t_1 + t_2, \qquad (7)$$

where t_1 is the traveltime τ_{sg} of the incident Rayleigh wave from the source **s** to **g**, t_f is the time τ_{sf} taken by this direct wave traveling from **s** to the fault **f**, and t_2 represents the traveltime $\tau_{sf} + \tau_{gf}$ of the Rayleigh wave arriving at the fault first and then scattered back

to **g**. Based on the property described by equation (7), it is able to migrate the original data using the natural Green's function by

$$m(\mathbf{x}') = \sum_{\mathbf{g}} d^{direct}(\mathbf{g}|\mathbf{s}) * d^{scatt}(\mathbf{g}|\mathbf{x}') e^{-i\omega 2\tau_{\mathbf{sx}'}}, \quad (8)$$

where the symbol * denote convolution of the filtered propagating waves d^{direct} from source to geophone, and the back-scattered waves d^{scatt} from the trial image point **x'** to geophone. These two waves are called natural Green's functions because they can be extracted by FK filtering. The image m in equation (8) can be obtained by picking up the convolved data at the listening time $2\tau_{sx'}$. Here, we only need a velocity distribution to obtain the final image from the convolved traces, but not to stack the back-scattered surface-wave data over trial quasi-linear curves. In Equation 8, the exponential term is not related to any receiver position so that it can be put out of the summation. Therefore, the summation over **g** in equation (8) becomes accurate because once a geophone captures the scattering signals from x', its local neighbors can do that as well, making all the convolved data show boosting amplitudes at a specific time $t = 2\tau_{sx'} = 2|x_s - x'|/v$, where v can be regarded as an average velocity from **s** to **x'**.

3. NUMERICAL RESULTS

3.1 SIMPLE Models

A 2D staggered-grid finite-difference elastic method (Virieux, 1986) is used to compute 100 shot gathers for the sources on the surface in the Figure 1(a) model. The data shown in Figure 1(b) were filtered and muted to only give the back-scattered arrivals (Figure 1(c)), and the filtered traces were migrated by equation 3 to give the prestack migration images depicted in Figure 3(a); stacking these prestack images gives the stacked migration image shown by Figure 3(b). The locations of the two faults are clearly delineated in the migration images. Based on this simple model, a modified model with non-vertical faults is presented in Figure 4(a), and its corresponding CSG #1 with source at the same position as Figure 1(b) is shown in Figure 4(b). Figures 1(b) and 4(b) present similar gathers so that migrating back-scattered surface waves is not limited to cases with vertical faults. Therefore, the back-scattered Rayleigh waves (Figure 4(c)) can still be obtained by muting, and migrating these waves in all CSGs produces the images depicted in Figure 4(d), which sum up to the stacked the image presented by Figure 4(e). Next, we focus more on migrating dispersive data in more realistic heterogeneous media (Halliday and Curtis, 2008).

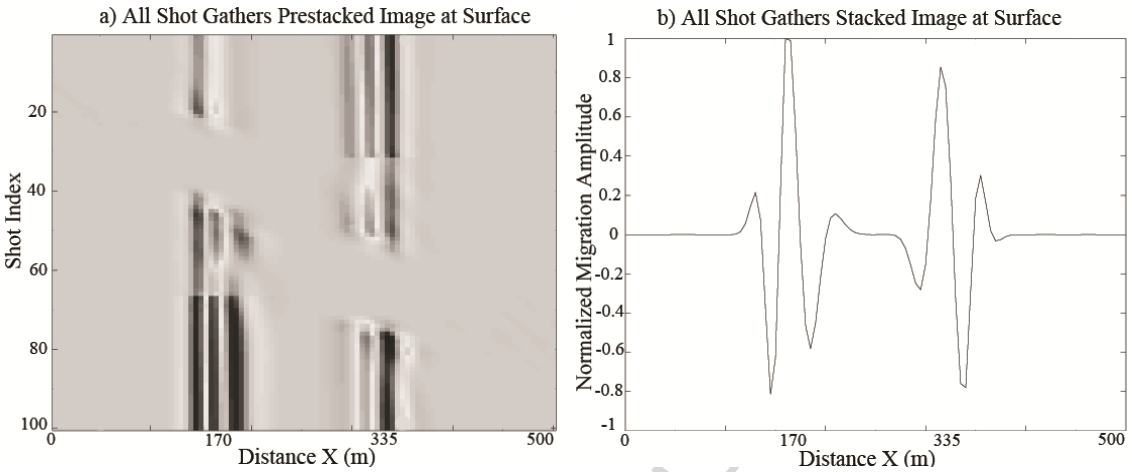

Figure 3: a) Prestack migration images obtained by migrating the back-scattered Rayleigh waves in 100 shot gathers, b) the stacked migration image along the surface of the model with two faults.

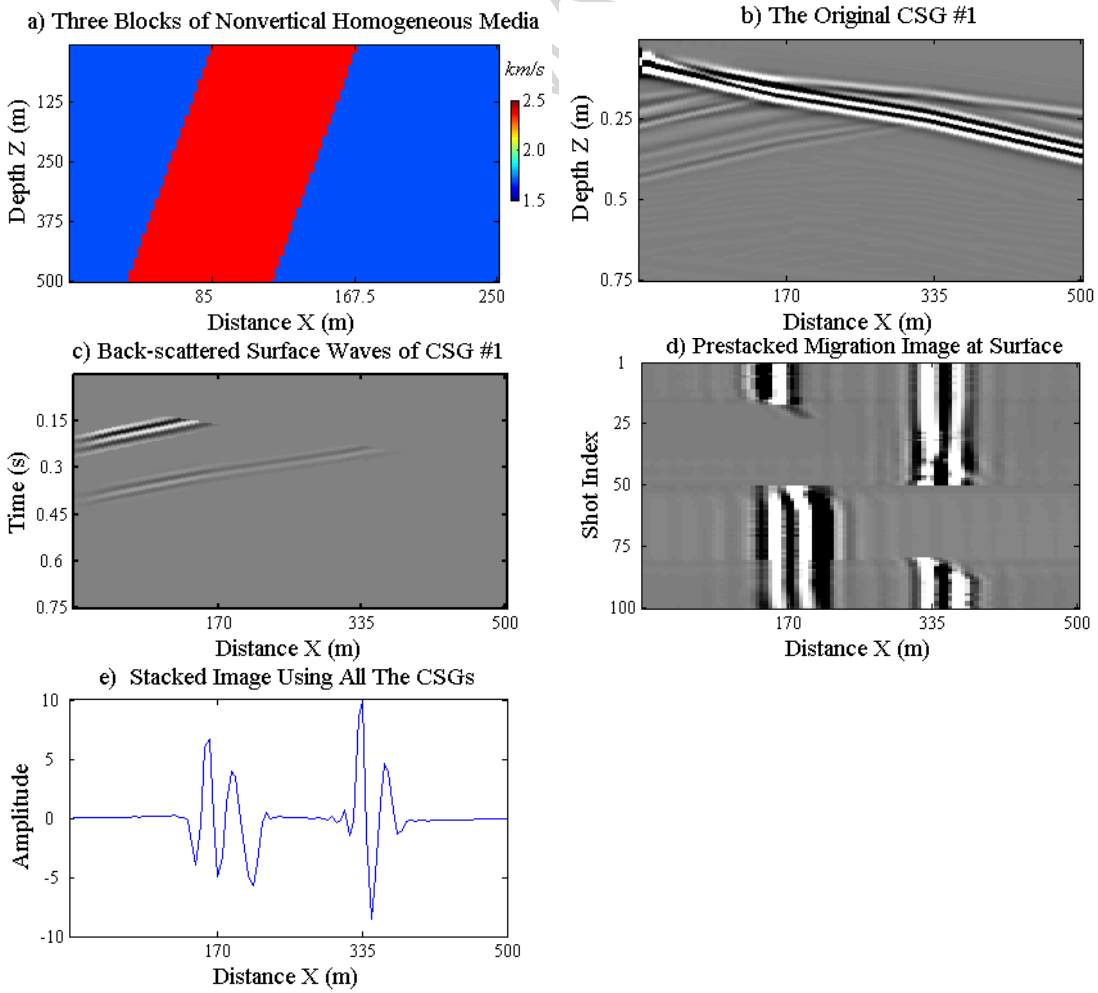

Figure 4: a) A non-vertical fault model, b) the CSG #1 generated based on this model, c) the muted back-scattered surface waves of CSG #1, d) the prestack migration images by

migrating the back-scattered Rayleigh waves from 100 shot gathers, and e) the stacked migration image along the surface of the model with two non-vertical faults.

3.2 MORE COMPLECATED MODELS

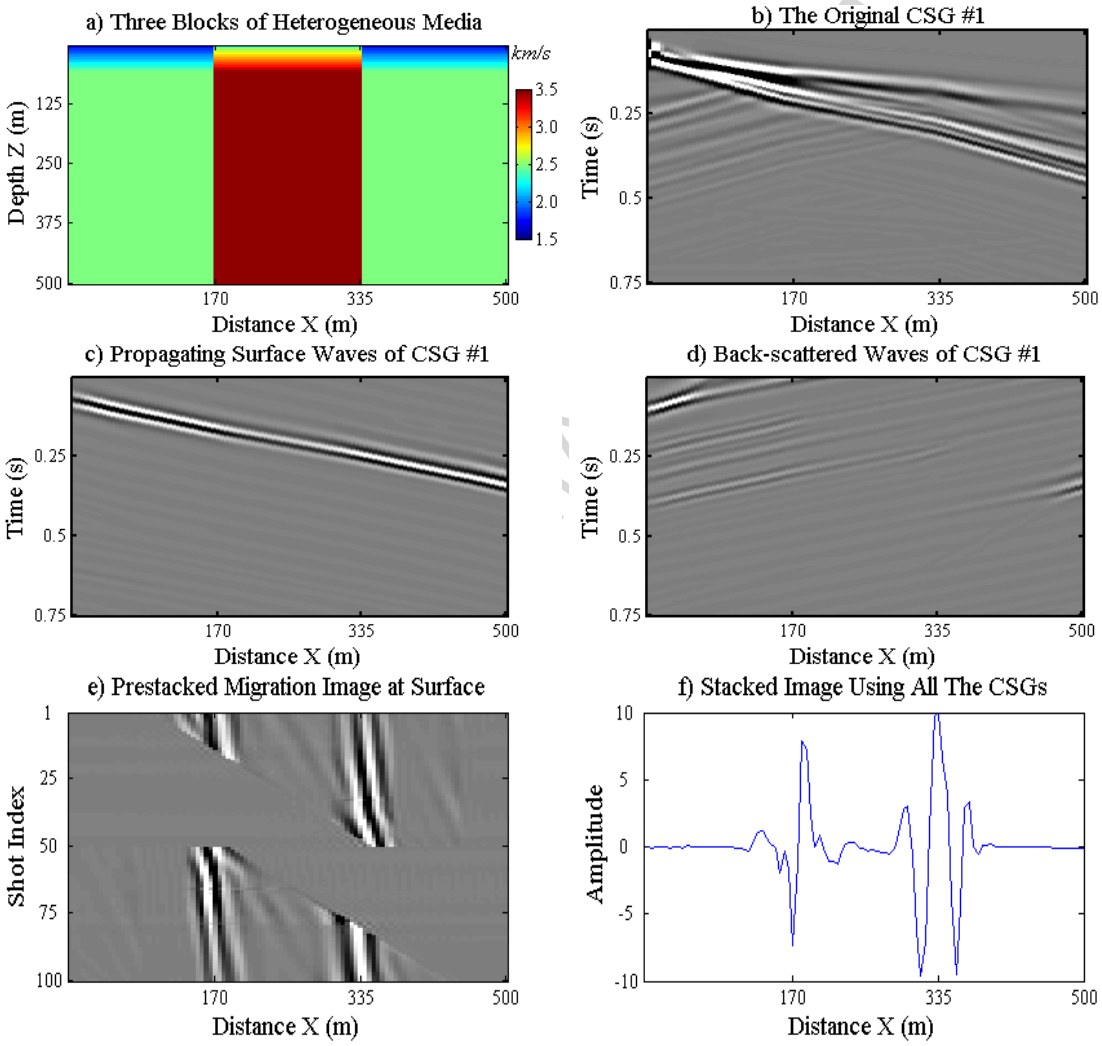

Figure 5: a) A three-blocked fault model with velocity variations near the surface, b) the CSG #1 generated based on this model, c) the filtered forward propagating Rayleigh waves of CSG #1, d) the filtered back-scattered surface waves of CSG #1, e) the prestack migration images obtained by migrating the back-scattered Rayleigh waves using 100 shot gathers, and f) the stacked migration image along the surface of the heterogeneous model with two faults.

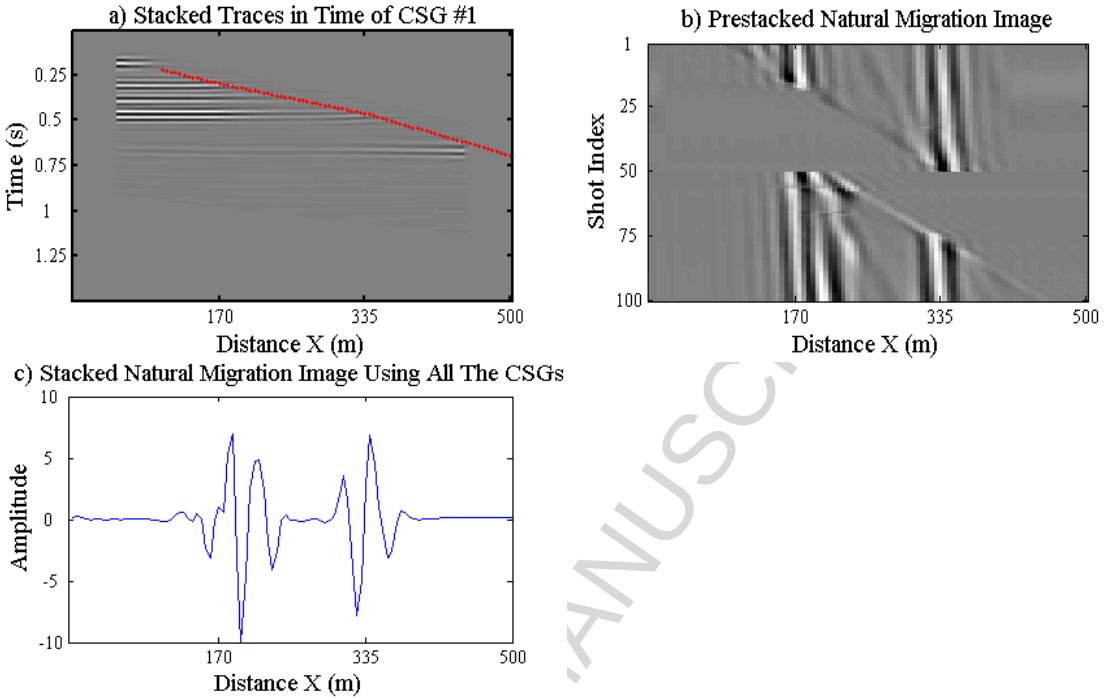

Figure 6: a) The stacked traces in time of CSG #1 for naturally migrating the back-scattered Rayleigh waves, b) the prestack natural migration images, and c) the stacked image.

Real seismic data with dispersive signals challenges the quality of imaging. To show the effectiveness of the methods proposed in the last section, we generate the data of dispersive surface waves based on the model shown in Figure 5(a). On the free surface, there are 100 receivers with a 5.0 *m* spacing and the shots are located at every receiver position. In this synthetic example, each CSG is recorded for 0.75 *s* with a sampling interval of 0.5 *ms*. As a typical shot gather, CSG #1 is presented in Figure 5(b). Waves of the same propagating velocities such as the forward and back-scattered Rayleigh waves are respectively F-K filtered out, and they are shown in Figures 5(c) and 5(d). After preprocessing the data, the regular migration method using diffraction stacking in Section 2.1 is firstly applied to the filtered data sets. Figures 5(e) and 5(f) show the prestack migration images and the stacked image, respectively. Secondly, the natural migration method is employed for imaging. Using the convolution operation in equation 8, the stacked traces associated with CSG #1 along time are presented in Figure 6(a). Note that waves of other types recorded before the direct Rayleigh wave are muted. It is reasonable because the velocity of the direct wave can be straightforwardly estimated from the data. Therefore, converting the Figure 6(a) to the prestack images is no more than repeatedly picking out images along the red "crosses" from figures like Figure 6(a) associated with every CSG using the estimated surface wave velocity distribution corresponding to the term $e^{-i\omega 2\tau_{sx'}}$ in equation 8. The final prestack and stacked images with the natural migration method are presented in Figures 6(b) and 6(c). Due to the influences of the strong energy from the sources, the near-offset signals become chaotic after filtering. Therefore, both the back-scattered and the forward propagating waves cannot be clearly discerned. Imaging these positions using near-offset traces is thus avoided. Compared

with Figure 5(e), there are still obvious artefacts in Figure 6(b) due to dispersions, but the fault images are straighter. Moreover, comparing the stacked images in Figures 6(c) with 5(f), the natural migration method can produce better image quality.

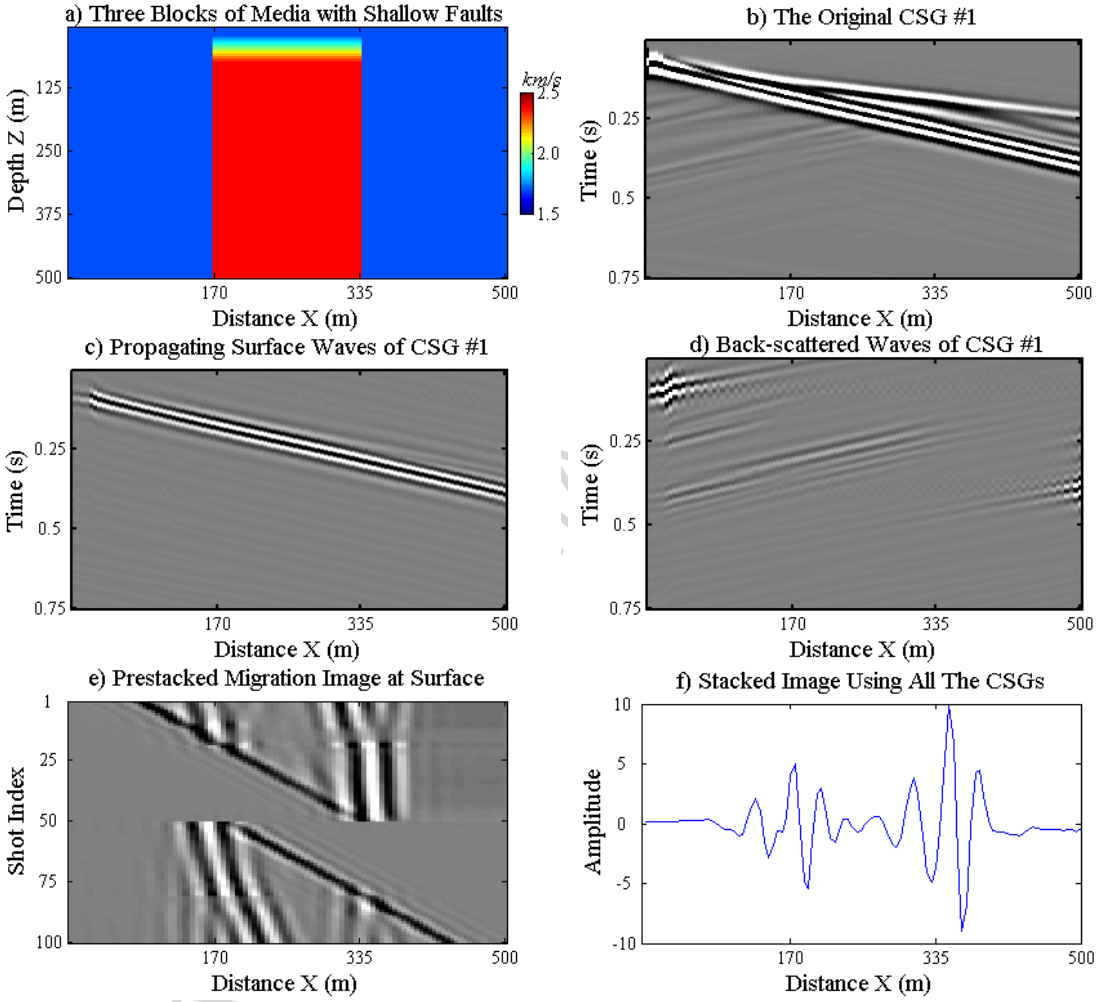

Figure 7: a) A three-blocked fault model with two near-surface faults, b) the CSG #1 generated based on this model, c) the filtered forward propagating Rayleigh waves of CSG #1, d) the filtered back-scattered surface waves of CSG #1, e) the prestack migration images obtained by migrating the back-scattered Rayleigh waves in 100 shot gathers, and f) the stacked migration image along the surface of the model with two shallow faults.

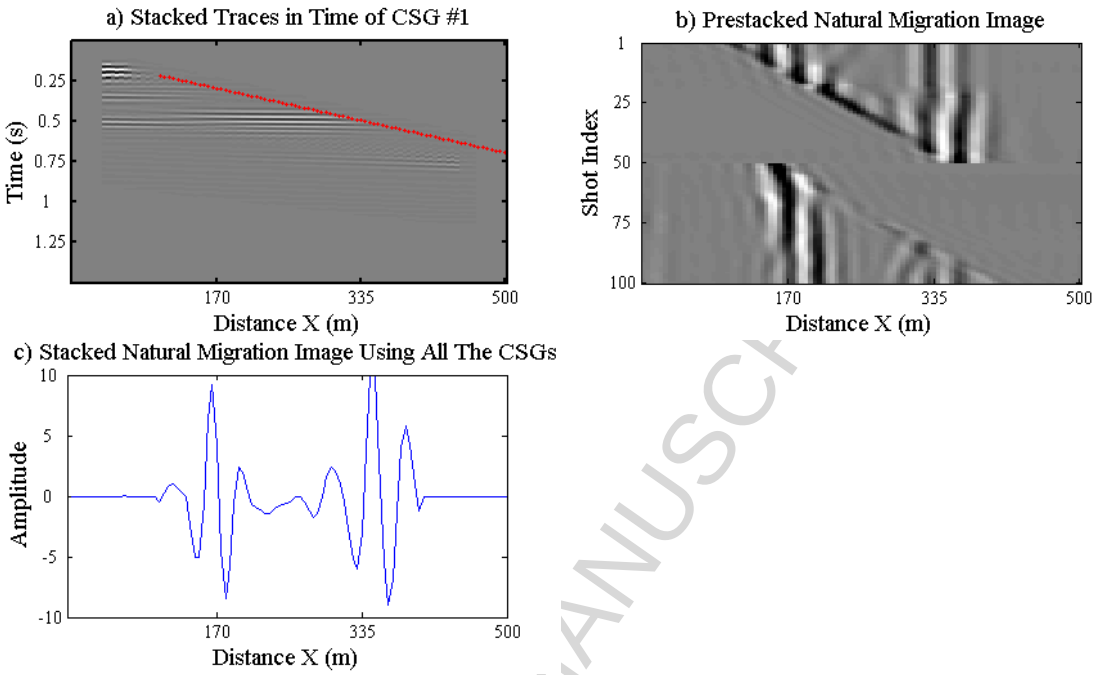

Figure 8: a) The stacked traces in time of CSG #1 for naturally migrating the back-scattered Rayleigh waves, b) the prestack natural migration images, and c) the stacked image.

Without changing the model size and acquisition geometry, the previous model is modified such that the two faults are buried within a distance of the source wavelength of the peak frequency (20 *hz*) under the ground, but not attached to the surface. Based on the model presented in Figure 7(a), CSG #1 is simulated and shown in Figure 7(b). Filtering the data set again shall we obtain the incident and the back-scattered waves, shown in Figures 7(c) and 7(d). The two methods are then repeatedly applied to the filtered data sets just as the previous example. Figures 7(e) and 7(f) show the migration results of the traditional imaging method with constant velocity, while Figures 8(a), 8(b), and 8(c) demonstrate the effects of natural migration method where the picking is along the straight line with red "crosses". By comparison, results of the natural migration method are not inferior to those of the traditional one. It is also concluded that near-surface faults can still be imaged from the data with appropriate sources. However, if the faults are buried deep such as in Figure 9(a), both methods may not work because no much fault information lives in the raw data set (Figure 9(b)), or the filtered back-scattered data (Figure 9(c)).

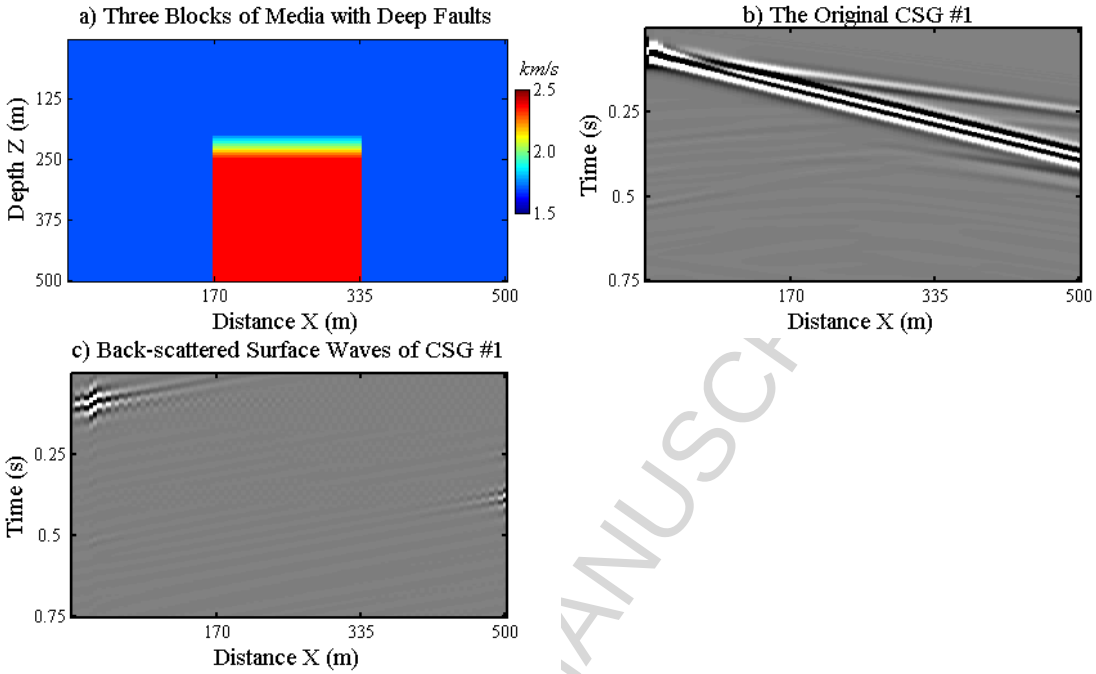

Figure 9: a) A three-blocked fault model with two faults buried in deep positions, b) the CSG #1 generated based on this model, and c) the filtered back-scattered surface waves of CSG #1.

3.3 A FIELD CASE

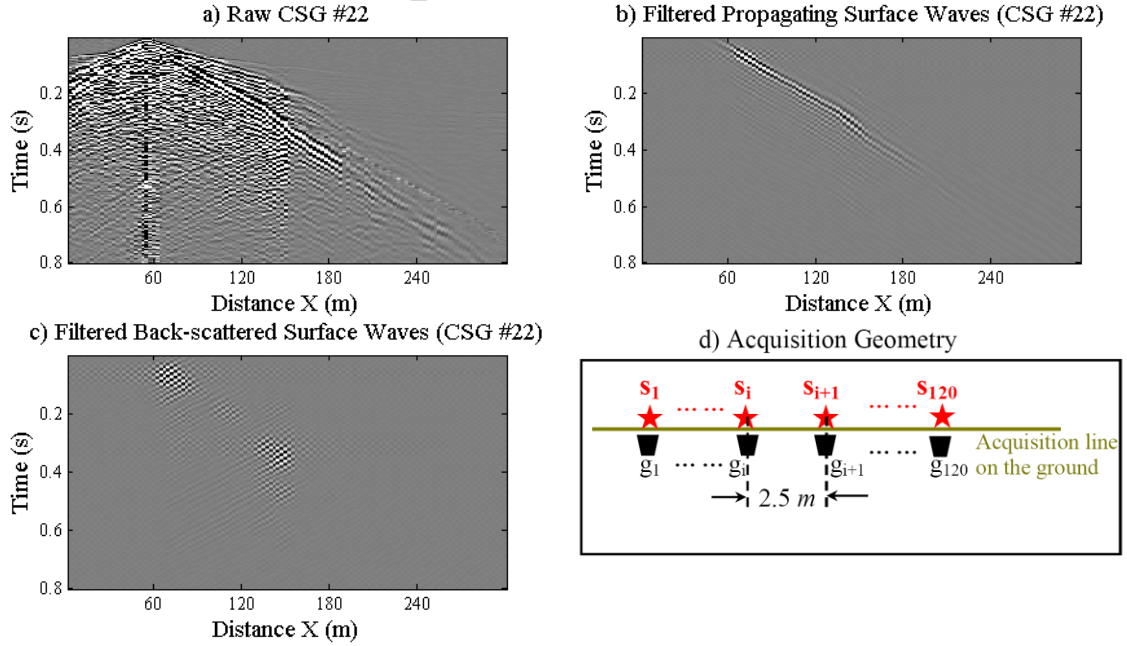

Figure 10: Raw data collected in Aqaba, Thuwal, Saudi Arabia, a) CSG #22, b) filtered propagating surface waves, c) filtered back-scattered waves in CSG #22, and d) the acquisition geometry for the field data.

In the field data example, the dispersions are not too strong so that we can focus on implementing the migration method straightforwardly. A total of 120 shot gathers were recorded near the Gulf of Aqaba in Saudi Arabia, where each shot gather contained 120 traces and the source and the receiver sampling intervals are both 2.5 *m*. A typical common shot gather is shown as an example in Figure 10(a). Shot gathers of propagating waves and back-scattered arrivals are respectively, FK filtered to isolate the forward going waves (mainly surface waves) and their corresponding back-scattered events shown in Figures 10(b) and 10(c). Figure 10(d) shows the acquisition geometry of the seismic line. First arrivals of pressure waves were picked and inverted to give the velocity tomogram in Figure 11(a). It shows the location of the two vaguely visible near-surface faults that break the surface at the position X = 150 m and just beneath the surface at X = 75 m. The common offset gather (COG) at the source-receiver offset of 0 *m* is shown in Figure 11(b); the COG has two distinct breaks in the reflector at the locations of the two faults in the tomogram, and another possible one in between, which at least indicates two fault locations that are consistent with those in the tomogram. The first half 60 CSGs are migrated while the second half 60 shot gathers are dropped owing to their unsatisfactory data quality.

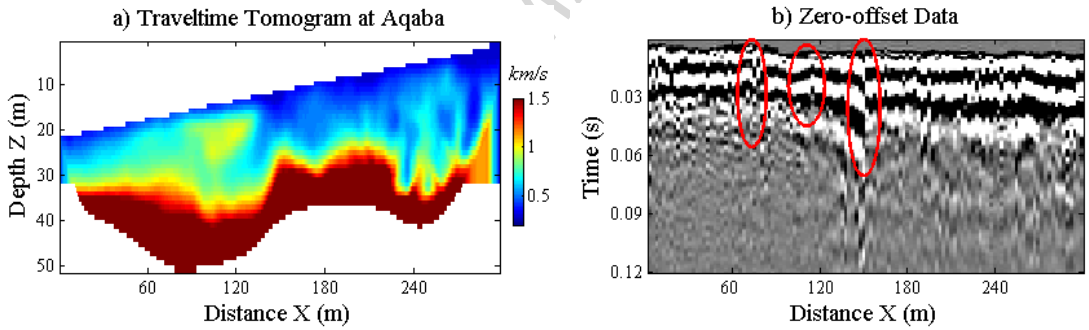

Figure 11: a) The traveltime tomogram inverted from Aqaba data, and b) the common offset gather with zero offset showing three possible faults circled by red ellipses.

Firstly, the back-scattered events are migrated only for the previous 60 shot gathers with constant velocity v = 300 *m/s* according to equation 3 to give the prestack migration images in Figure 12(a) and the stacked migration image in Figure 12(b). Secondly, we use a velocity scan technique to measure the weights of several velocities at every position along the acquisition line. For instance, we fix the 31st receiver position, and then scan the filtered CSG #5 at sequentially trial time moments shown in Figure 13(a) with several trial velocities from v = 240 m/s to 420 m/s for obtaining their weights. Therefore, we can estimate the most suitable velocity at that position (see Figure 13(b)) after scanning all the filtered CSGs. The scanned velocity distribution for migration is labeled by black crosses in Figure 13(b), which is calculated from mass point pinpointing technique of an object in physics. With this scanned version velocity, the prestack migration image (Figure 13(c)) shows some improvement in that the events from shots #21 to #40 become more continuous and straight, while images migrated from the first 20 shots are still a little obscure. The stacked images in Figures 12(b) and 13(d) are somewhat identical by both showing the two faults in the tomogram Figure 11(a) but not

the possible one although there are clear events between them in the prestack images (see Figures 12(a) and 13(c)).

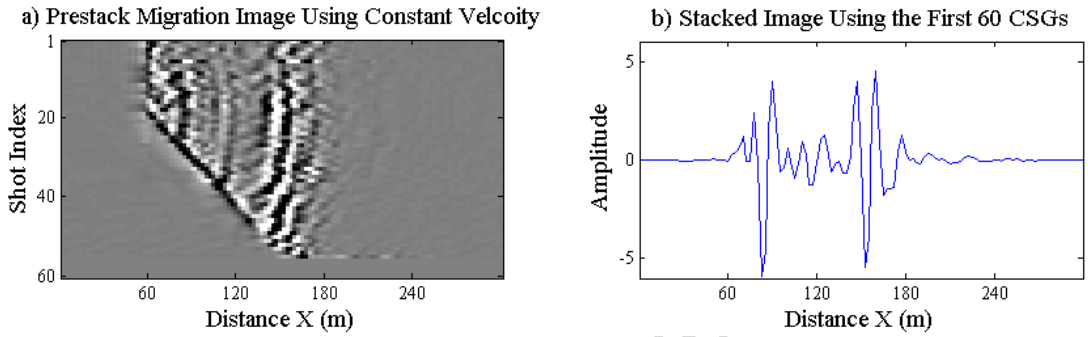

Figure 12: a) Prestack migration image using constant velocity = 300 m/s, and the b) stacked migration image.

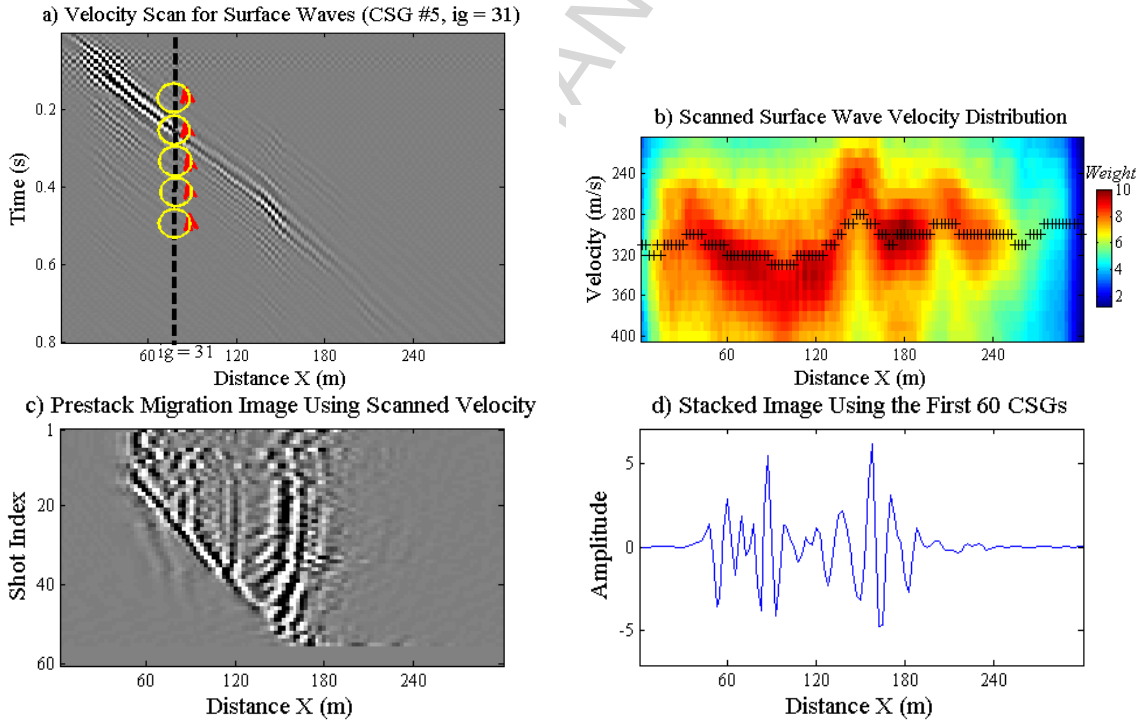

Figure 13: a) Technique of velocity scan applied to the filtered propagating surface waves, b) a scanned surface wave velocity distribution with black crosses labeling migration velocity along the seismic line, c) the prestack migration image using the scanned velocity, and d) the stacked image.

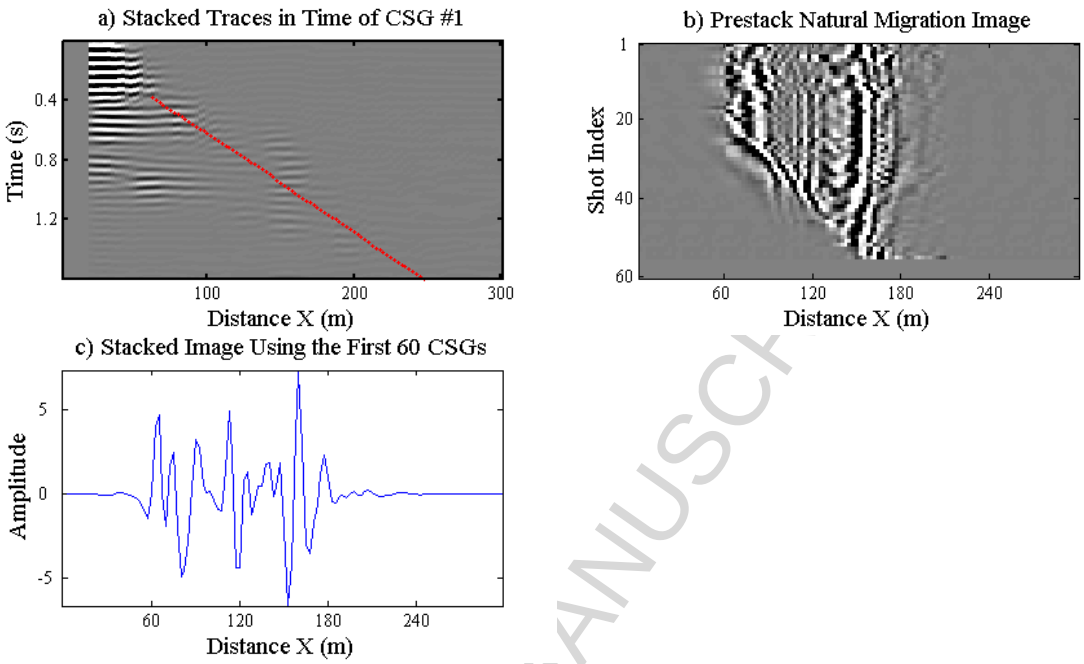

Figure 14: a) The stacked traces in time of CSG #1 for natural migration, b) the prestack migration image using natural Green's functions, c) and the stacked image.

Finally, we migrate the data set with natural Green's function. The stacked traces in time of CSG #1 with a line of red "crosses" for imaging (Figure 14(a)) show that it is also possible to migrate field data using natural Green's functions. The prestack images of all CSGs are presented in Figure 14(b). It shows acceptable and competitive quality in contrast to Figures 13(c) and 12(a) with continuous events especially for the first 15 shot gathers. Moreover, these interpreted fault locations in the stacked image Figure 13(c) agrees with those indicated in the first-arrival traveltime tomogram and zero-offset COG shown in Figure 11(b).

4. CONCLUSIONS

We show that diffraction stack migration can be used to directly map the distribution of near-surface faults. Unlike the indirect method of detecting discontinuous reflectors in a stacked reflection section, the direct method simply isolates the back-scattered surface waves and migrates them to their place of origin along the fault plane. The key assumption is that near-surface faults generate detectable back-scattered surface waves from impinging surface waves. Instead of summing events along trial hyperbolas, surface wave migration sums events along trial quasi-linear trajectories that correspond to the one-sided moveout of back-scattered surface waves. Based on this imaging technique, the natural migration method is proposed that utilizes the traveltime property of the forward and back-scattered Rayleigh waves and avoids some artefacts in summing the fault events. In the synthetic examples, the migration is easily implemented and the feasibility of the methodologies is directly proved. First, trivial tests are successfully carried out on imaging vertical and non-vertical faults in the three blocks of homogeneous media. Secondly, results in the heterogeneous media validate the effectiveness of the natural

migration method, with the image quality not inferior to that by the previous method which relies on a velocity distribution in events summation. Moreover, it is also shown that these methods also apply to imaging geological structures with shallow faults. However, if the faults are buried too deep, imaging using reflection and diffraction waves is more pertinent with the assumption that the upper end of the fault serves as a diffractor. In the land data case, where weak dispersive arrivals are ignored and many of them are suppressed by filtering, two velocity profiles are firstly used to migrate the filtered back-scattered surface waves. The scanned velocity distribution shows some advantage over the constant one for this method. We lastly propose a natural migration method using Green's functions that can be directly extracted from the data. It does not need any velocity information to stack events at fault locations, other than a general velocity distribution for the final prestack image. The major artifacts in this work may come from two parts: the filtering operation and the dispersive waves. In the F-K filtering process, we have manually lengthened the listening time and acquisition offset of the 2D data so that the F-K filter causes fewer artefacts. Strong dispersions may cause strong artefacts in the final images. In the synthetic and the field examples in this work, the dispersions are not strong to affect the final results. But if they are very strong, necessary de-dispersion operations should be applied prior to imaging.

We can now migrate back-scattered surface waves, which are among the strongest signals in a shot record, to directly detect the presence of faults that are just below the surface or hidden by foliage. Applying this method to global seismic data or passive exploration data that have been interferometrically processed might open new opportunities in mapping tectonic features over the extent of the array. This is especially true with passive seismic data where it is very easy to generate virtual surface waves but hard to generate virtual reflections. It deserves to notice that this method is not only limited to vertical faults, but also applies to non-vertical faults just as the synthetic and the land cases above. As long as the back-scattered surface wave can be detected and separated, the migration with and without velocity profiles can be carried out similar to the numerical examples in this study. The current method is mainly applicable to the 2D or 2.5D cases, and caution should be exercised for interpretation because a fault, a topography variation, or a near-surface impedance anomaly can all generate back-scattered surface waves. To alleviate this interpretation ambiguity, back-scattered surface wave migration in 3D data is under research so that long linear features in the migration image are likely to indicate linear faults, rather than isolated impedance anomalies.

ACKNOWLEDGMENTS

We thank the sponsors of the CSIM Consortium (http://csim.kaust.edu.sa/web/) for their support. We also thank Prof. Gerard T. Schuster and anonymous CSIM members for their efforts and comments in the development of this work. This work is also sponsored by the National Natural Science Fund of China (Grant No.: 11501302, 61571238, 61571233, 61501250), the Natural Science Foundation for Young Scientists of Jiangsu Province (Grant No.: BK20150856, BK20140879), and the Scientific Research Foundation of Nanjing University of Posts and Telecommunications (NUPTSF, Grant No.: NY214170).

References

Aki, K., and P. Richards, 1980, *Quantitative seismology*: W. H. Freeman & Company.

Blonk, B., and G. C. Herman, 1994, Inverse scattering of surface waves: A new look at surface consistency: Geophysics, **59**, 963–972, http://dx.doi.org/10.1190/1.1443656.

Campman, X. H., K. Wijk, J. A. Scales, and G. C. Herman, 2003, Suppression of near-field scattered surface waves: 65th Conference & Exhibition, EAGE, Extended Abstracts, P078.

Halliday, D., and A. Curtis, 2008, Seismic interferometry, surface waves and source distribution: Geophysical Journal International, 178, 1067-1087.

Luke, B. and C. Calderón-Macías, 2008, Scattering of surface waves due to shallow heterogeneities: 78th Annual International Meeting, SEG, Expanded Abstracts, 1283–1287.

Schuster, G. T., S. Hanafy, and Y. Huang, 2012, Theory and feasibility tests for a seismic scanning tunneling macroscope: Geophysical Journal International, **190**, no. 3, 1593–1606, http://dx.doi.org/10.1111/j.1365-246X.2012.05564.x.

Snieder, R. K., 1986, 3D Linearized scattering of surface waves and a formalism for surface wave holography: Geophysical Journal of the Royal Astronomical Society, 84, 581–605.

van Wijk, K., 2002, Multiple scattering of surface waves: Ph.D. dissertation, Colorado School of Mines.

Virieux, J., 1986, P-SV wave propagation in heterogeneous media: Velocity-stress finite-difference method: Geophysics, 51, 889–901, http://dx.doi.org/10.1190/1.1442147.

Yu, H., B. Guo, S. Hanafy, F. Lin, and G. T. Shuster, 2014. Direct detection of near-surface faults by migration of back-scattered surface waves: The 84th SEG annual meeting in Denver 2014, SEG Technical Program Expanded Abstracts 2014, pp. 2135-2139.

Highlights

- Back-scattered surface waves are used to detect various unseen faults.
- Natural Green's functions from the data are utilized in the imaging condition.
- Neither exact velocity nor source wavelets are required for the migration.
- The migration quality validates the methodologies in detecting faults.